Metal-Organic Frameworks with Two Different Metal Centers for Thiophene Adsorption: Synthesis, Characterization and Mechanism Analysis

Yatao Wang,[1] Peng Zhang,[2] Hongjuan Li,[1] Qiuju Xu,[2] Shujun Liu,[1] Xiaopeng Liu,[2] Xuehua Guo,[1] Yitao Li,[1] Jinzhang Liu,[2] Sen Dong,[1,*] Zhi Wei Seh,[3,*] Qianfan Zhang, [2,*]

1 Coal Chemical R&D Center of Kailuan Group, Tangshan, Hebei Province, 063018, PR China,

2 School of Materials Science and Engineering, Beihang University, Beijing 100191, PR China,

3 Institute of Materials Research and Engineering (IMRE), Agency for Science, Technology and Research (A*STAR), 2 Fusionopolis Way, Innovis #08-03, Singapore, 138634, Republic of Singapore

*Corresponding authors: ecds@kailuan.com.cn (S. Dong), sehzw@imre.a-star.edu.sg (Z.W. Seh), qianfan@buaa.edu.cn (Q. Zhang).

Abstract

Thiophene, widely found in fossil fuels, not only corrodes equipment but also causes great harm to the environment after combustion. Adsorptive desulfurization can deeply desulfurize fuels with low sulfur content and shows great development prospect. We experimentally studied the adsorption of thiophene and benzene in Cu-BTC and two types of IZE metal-organic frameworks (MOFs). By changing the temperature and concentration conditions, we compared the separation performance of MOFs with different metal centers. We found IZE-1 to have excellent s high thiophene adsorption capacity selectivity for thiophene adsorption at low thiophene concentration and (-up to 9.3 mg S/g MOF at 70℃), superior to that of Cu-BTC. We performed first-principles calculations and elucidated the mechanism of thiophene adsorption by analyzing the electronic structure of MOFs. The molecular dynamics simulation further explains the high selectivity of thiophene adsorption and the adsorption process. This study

demonstrates the potential for MOFs to be used in thiophene adsorption, particularly at high thiophene concentrations.

Keywords: Thiophene Adsorption; Metal-Organic Frameworks; Separation Performance.

1. Introduction

The petrochemical industry is facing increasingly stringent environmental mandates to remove sulfur-containing compounds in fuels and also requires the production of sulfur-free clean fuels [1,2]. Conventional hydrodesulfurization (HDS) is an effective method for removing mercaptan, thioether and other aliphatic S compounds but not for thiophene and its derivatives[3]. Sulfur-free fuels are difficult to produce because excessive hydrogenation saturates the aromatics and greatly reduces the octane rating[4]. Therefore, developing ultradeep desulfurization technologies is urgently needed to meet environmental regulations.

Adsorptive desulfurization (ADS) is a promising ultradeep desulfurization technology due to its ambient operating conditions and high selectivity for removing thiophene compounds, leaving fuel unchanged[5,6]. The mechanism of adsorption desulfurization is mainly consisted of hydrogen bond, π-complexation, van der Waals force and sulfur-metal (S-M) bond between metal and sulfur compounds[7]. Among them, the interaction mechanism such as π-complexation, hydrogen bond and S-M bond can directly influence the desulfurization performance[8-10]. Although π-complexation greatly increased the adsorption capacity of thiophene and its derivatives, the adsorption capacity of aromatics (about 30% in fuels) might decrease in the presence of thiophene (kinetic diameter of 4.6 Å) because of competitive adsorption, such as benzene (kinetic diameter of 5.8 Å)[11]. On the contrary, the adsorbents based on S–M bond have high adsorption selectivity in removing thiophene and its compounds along with aromatics[12,13].

MOFs with the crystalline porous feature are formed by metal ions or metal clusters and organic ligands connected through self-assembly[14,15]. MOFs show great

potential in separation and have become a hot topic for research, particularly in the area of high selective adsorption of the trace of sulfur-containing compounds in fuels[16-18]. In general, the metal in the center and the chemical functional groups over the surfaces of MOFs can be customized to improve their stability and recyclability. Wang et al. used Ni-doped Cu-BTC to remove thiophene in simulated oil, with higher stability and selectivity for thiophene after modifying the doped MOF[19]. Liu et al. modified Fe_3O_4/HKUST-1 with graphite oxide for desulfurization, increasing capacity and the reusability from the unmodified form by 24% and 10% respectively[7]. These studies changed the structure and properties of MOFs by respectively introducing double-coordinated metals and graphene oxides but did not study the relationship between MOF microstructure and adsorption performance. Notably, in a study conducted by Li et al.[20], ultradeep desulfurization from model gasolines was explored through an adsorptive approach. Various porous materials exhibiting promising ultradeep desulfurization capacities (N thiophene $\geq$ 0.1 mmol/g) were identified, including Zn-BDC, MOF-70, MOF-69C, UIO-66, Cd_3BTB_2, ZIF-77, and ZIF-69. However, it is important to emphasize that the aforementioned materials were only able to achieve this performance at 298 K and 10 kPa. Therefore, the mechanism with structural analysis of MOFs on the thiophene adsorption performance has not been deeply explored.

In our previous studies, high-performance MOFs were extracted from ~12020 candidates in the database which possess the strongest adsorption strength based on first-principle calculations[21]. In this study, our selection of IZE-1, IZE-2, and Cu-BTC as the focal MOF materials was grounded in their demonstrable computational promise, the strategic alignment of central metal atoms and ligands, and the imperative for controlled experimentation to underscore the pivotal role of the central metal atom in thiophene adsorption. Our work is the first to use the prepared IZE-type MOF for thiophene adsorption and can achieve excellent adsorption performance with the adsorption amount of thiophene larger than 0.11 mmol/g at the high temperature of 343

K and the normal pressure of 0.1 kPa. We also used first-principles calculations and combined molecular dynamics simulations to evaluate their dynamic and thermodynamic stabilities. This study provides guidelines for rational experimental adsorption of thiophene

2. Experimental section

2.1.Materials

Zinc nitrate hexahydrate ($Zn(NO_3)_2 \cdot 6H_2O$, 98%), N, N-dimethylformamide (DMF) and dimethylsulfoxide (DMSO) were supplied by Adamas (Shanghai, China). 1, 1′-Ethynebenzene-3, 3′, 5, 5′-tetracarboxylic acid (H_4EBTC) was prepared following published methods[22]. Benzene, thiophene and 1, 3, 5-trimellitic acid were supplied by Adamas (Shanghai, China). Copper nitrate trihydrate and Nitric acid were obtained from Aladdin Holdings Group Co., Ltd (Shanghai, China). All chemicals were analytical grade and not further purified. Deionized water obtained from the up-water purification system was purchased from Chengdu You Pu Biotechnology Co. Ltd. for this study. All reagents were of analytical grade and used without further purification.

2.2.Synthesis of Cu-BTC and IZE-1/2

Synthesis of Cu-BTC: the reaction was carried out by the hydrothermal method. The reactants $Cu(NO_3)_2 \cdot 3H_2O$ (1.087 g) and 1, 3, 5-trimesic acid (0.525 g) were ultrasonically dissolved in 15 mL of ethanol. This was added to 15 mL of ultrapure water in a reaction kettle and incubated in a high-temperature oven for 14 h. The blue crystal produced was suction filtered and dried in vacuum at 80℃ for 24 h to obtain a blue powder.

Synthesis of IZE-1: ethynyl biphenyl-3, 3', 5, 5'-tetracarboxylic acid (50 mg) and $ZnSO_4 \cdot 6H_2O$ (150 mg) were added to a glass bottle. The mixture was ultrasonicated for 20 mins until all reactants had dissolved. After 0.6 mL of nitric acid was added to the solution, the glass bottle was sealed and incubated in a high-temperature oven at 85°C for 12 h. After cooling to room temperature, the precipitate was separated by suction filtration, rinsed three times with DMF and ethanol, and dried in vacuum at 60°C to

obtain IZE-1(Fig. S1).

Synthesis of IZE-2: We mixed 50 mg ethynyl biphenyl-3,3',5,5'-tetracarboxylic acid (0.14 mmol), 150 mg zinc nitrate hexahydrate (0.5 mmol) and 25 mg 5-amino isophthalic acid (AIP) (0.14 mmol) in a glass bottle containing 2 ml DMF and 2 ml DMSO. The contents were ultrasonicated for 10 min until all reactants were dissolved. The glass bottle was then sealed and incubated in a high-temperature oven at 85°C for 10 h. After cooling to room temperature, the precipitate was obtained by suction filtration with washes using DMF and ethanol. This precipitate was dried in vacuum at 60°C to obtain IZE-2.

2.3. Characterization

A field emission scanning electron microscopy (FESEM, JEOL-7800F, Japan) was employed to study the morphology and size of MOF particles. The crystal structure of the samples was analyzed by using X-ray diffraction (XRD, Bruker, Germany) measurements at a scanning rate of 10°/ min based on Cu Kα radiation (λ = 1.5406 Å). The N_2 adsorption–desorption isotherm of the particle was measured by the ASAP 2020 Surface Area and Porosity Analyzer (Micromeritics Instrument Corp, USA) at 77 K. The specific surface area and pore size distributions were calculated by using the Brunauer−Emmett−Teller (BET) equation and Barrett-Joiner-Halenda (BJH) equation, respectively. The thermal stability of the particle was determined by a thermogravimetric analyzer (Mettler Toledo, USA) with a heating rate of 10℃/min in a nitrogen atmosphere.

To elucidate the mechanism of thiophene adsorption, first-principles calculations were performed by applying the plane-wave-based density functional theory (DFT) method implemented in the Vienna Ab-initio Simulation Package (VASP)[23,24]. The projector augmented wave (PAW) pseudopotentials were used to describe the ion-electron interaction. The generalized gradient approximation (GGA) was parametrized by the Perdew-Burke-Ernzerhof (PBE) exchange-correlation functional to analyze the exchange-correlation[25]. The cut-off energy for the plane was set to 450 eV, with an error

of less than 1 meV per atom. The Brillouin zone was sampled with a 3 × 3 × 3 k-mesh using the Gamma-centered Monkhorst-Pack scheme. The Fermi-smearing method was applied with 0.08 eV smearing width. The convergence criteria of the total energy was set to 10^{-5} eV while all ions were relaxed to a force tolerance less than 0.01 eV/ Å. Van der Waals (VdW) interactions between atoms and molecules were evaluated by the "zero damping" DFT-D3 parameter of Grimme. And the whole structure underwent the ab initio molecular dynamics (AIMD)[26] simulation for 25 ps to ensure that the equilibrium was reached. During AIMD simulation, NVT ensemble at 300 K was adopted with Nose mass parameter being set to 0.5 to control temperature oscillations.

The adsorption energy (ΔE_{ads}) of one thiophene molecule is defined as Eqs. (1):

$$\Delta E_{ads} = E_{MOF/Thiophene} - (E_{MOF} + E_{Thiophene}) \quad \text{Eqs. (1)}$$

Where E_{MOF}/Thiophene is the total electronic energy of the MOF with one thiophene molecule adsorbed, MOF is the total electronic energy of the bare MOF, and $E_{Thiophene}$ is the total electronic energy of a free thiophene molecule. A more negative ΔE_{ads} value indicates stronger adsorption, the corresponding MOF being the active sorbent for thiophene.

2.4. Experiments of static adsorptive desulfurization

The IZE material was vacuum-dried overnight at 80 °C for 15h to remove adsorbed water and other volatile pollutants. Then, 40 mg of a sample (Cu-BTC/IZE-1/IZE-2) was added to 10 g of thiophene/benzene mixture containing different concentrations of thiophene. Next, the mixture was heated at 60 °C under intense stirring, and a small amount of liquid was removed after every specified time. Finally, the above-mentioned liquid samples were analyzed by a compact sulfur and nitrogen analyzer (Analytik Jena, Germany) to determine sulfur content.

The sulfur and nitrogen element analyzer was used to analyze the content of sulfide thiophene in the oil phase of raw materials and adsorption products. The temperature was programmed at a heating rate of 10 °C/min to the furnace temperature of 1100 °C and kept for 3 mins. The external standard method was used to quantitatively analyze

the thiophene content of raw materials and adsorption products and the following formula was used to calculate the thiophene content in Eqs. (2):

$$c_s = \exp\left[\frac{\ln c_2 - \ln c_1}{\ln A_2 - \ln A_1}\left(\ln A_t - \ln A_1\right) - \ln A_1\right] \quad \text{Eqs. (2)}$$

A_t is the peak area of thiophene when the sample is tested for further analysis; A_1 and A_2 are the peak area of thiophene when the standard sample is analyzed; c_1 and c_2 are the concentration of the standard solutions, respectively.

3. Results and discussion

3.1 Characterization of the adsorbents

SEM images of the two types of Zn-BTC prepared under different conditions (IZE-1 and IZE-2) indicated differences in size and shape (Fig. 1). IZE-1 formed elongated polyhedrons of uniform size (from 3 to 5 μm), while IZE-2 formed smaller particles that beneficially increased the specific surface area of the MOF. This strongly indicates that Zn-BTC MOFs prepared with different solvents result in differing morphologies and stacking methods. The hexagonal particles of Cu-BTC with similar size as IZE MOFs was showed in Fig. 1c.[27,28]

The nitrogen adsorption-desorption isotherms for Cu-BTC are presented in Figure S1. The Cu-BTC isotherms demonstrate Type-I characteristics, exhibiting a rapid ascent at low relative pressures followed by a plateau, indicative of its micro-porous structure[29]. The BET surface area of Cu-BTC is measured at 1190.8 m^2/g, and the ultimate adsorption is contingent upon the available micro-pore volume. For the IZE-type MOF materials, the adsorption curves exhibit S-shaped isotherms, corresponding to the occurrence of a reversible single-layer adsorption process either on the surface of non-porous solids or on solids with large pores. In the low P/P_0 region, the curve concaves upward or downward, reflecting the strength or weakness of the interaction between the adsorbate and adsorbent. A turning point is observed at low P/P_0 values, marking the first steep segment of the isotherm, indicating saturation adsorption of the

monomolecular layer. With increasing relative pressure, a second layer begins to form, reaching infinite layers at the saturation vapor pressure, signifying this type of isotherm. Such isotherms are often encountered when the pore size of the adsorbent exceeds 20 nm, with no upper limit to the solid pore size. Calculations reveal that the specific surface areas of IZE-1 and IZE-2 surpass that of Cu-BTC, while both IZE-1 and IZE-2 exhibit narrower pore size distributions centered around 15 nm and 25 nm, respectively, which are also higher than that of Cu-BTC.

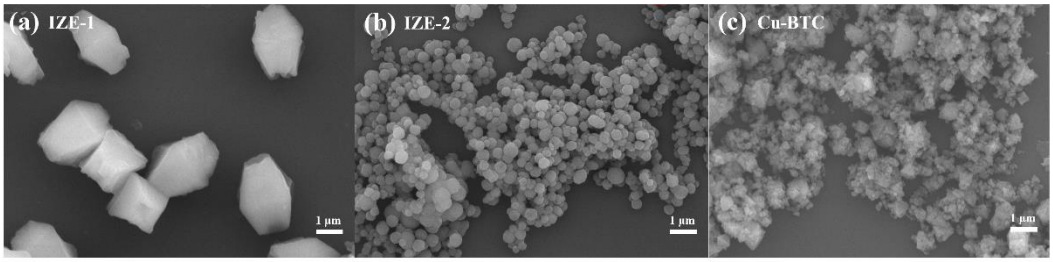

Figure 1. FESEM images of (a) IZE-1, (b) IZE-2, and (c) Cu-BTC.

We also analyzed the X-ray diffraction (XRD) spectra for the three MOFs to ascertain if the MOFs were correctly prepared. For both IZE-1 (Fig. 2a) and IZE-2 (Fig. 2b), the spectra (black) agreed well with the standard XRD characteristic peak (red), indicating that the structures of the IZE particles conformed to the standard characteristic structure[30]. The spectrum for the Cu-BTC particle (Fig. 2c) showed the characteristic diffraction peaks to be roughly similar to that of the simulated Cu-BTC[31,32]. The diffraction peaks at 2θ=6.6°, 9.5°, 11.6°, 13.4°, 17.4°, and 19.0° corresponded to the (200), (220), (222), (400), (333) and (440) crystal planes of Cu-BTC. These results proved our successful synthesis of Cu-BTC and IZE. The difference in the relative intensity diffraction peak from that of the simulated calculation was due to the simulated Cu-BTC having complete crystal structure without impurities.

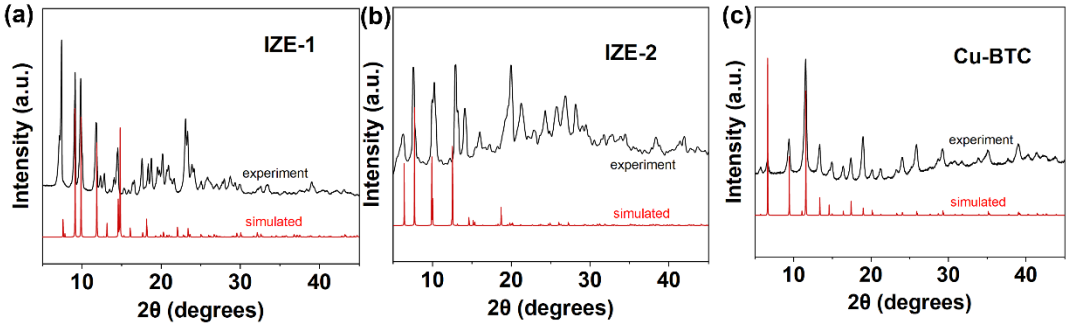

Figure 2. XRD patterns of (a) IZE-1, (b) IZE-2, (c) Cu-BTC.

The stability of three MOFs was determined by thermogravimetric (TG) analysis (Fig. 3). There were two main stages of weight loss on the TG curves for all three MOFs. IZE-1 (Fig. 3a) loses 39.3% of its mass from room temperature to 360°C which corresponds to the simulated structure of [Zn_2(EBTC)], with each unit corresponding to 2 coordinated H_2O, 5.5 guest coordination molecules H_2O and 2.5 guests DMF molecules. The weight loss during the first stage was 39.8% which was consistent with the simulated structure, with the backbone of IZE-1 starting to break down with increasing temperature. IZE-2 (Fig. 3b) experienced a similar weight loss of 39.0% in the temperature range of 25°C to 253°C during the first stage. Each unit of [Zn_2(EBTC)] corresponds to 2 coordinated H_2O, 10.5 guest molecules H_2O, 0.5 guest molecule DMF and 0.5 guest molecule DMSO (calculation result in 38.5%). As all the coordinated water molecules and guest solvent molecules in the MOFs break down, they all decompose immediately. For Cu-BTC (Fig. 3c), ~ 5% of the weight loss occurs in the temperature range around 40–100°C, which could be attributed to the evaporation of the adsorbed water. The second step of weight loss started at ~280°C and ended at ~340°C, which was induced by the decomposition of the organic ligand skeleton and the transformation of the MOF into copper oxide.

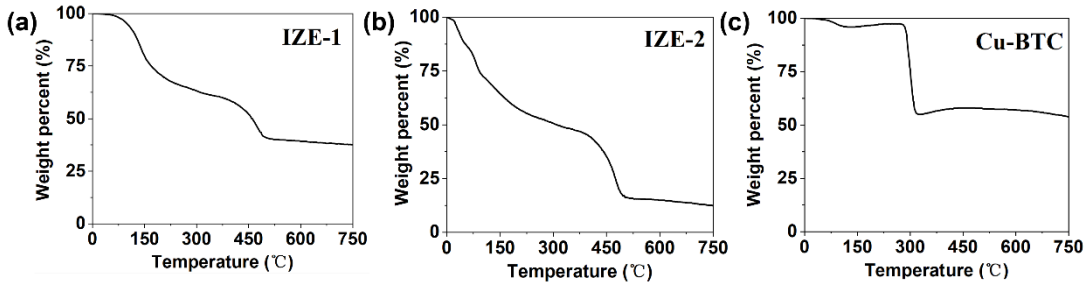

Figure 3. TG curves of (a) IZE-1, (b) IZE-2, (c) Cu-BTC.

3.2 Static adsorption performance of Cu-BTC, IZE-1 and IZE-2

We studied the desulfurization performance for IZE-1, IZE-2 and Cu-BTC at low thiophene concentrations of 1 ppm and 17.5 ppm. At the adsorption temperature of 60°C, the thiophene remaining in the thiophene/benzene mixture was measured as a function of time (Fig. 4). During the first 10 mins, all three MOFs showed rapid thiophene adsorption. After 20 mins, this adsorption increased slowly and gradually reached equilibrium. The concentration of thiophene in the thiophene/benzene mixture was reduced from 17.5 ppm to 25.3 ppb or less, with both IZE-1 and IZE-2 able to adsorb enough thiophene to keep its concentration about half of that for Cu-BTC. Although the results indicated that all three types of MOFs can rapidly and completely adsorb thiophene when it is present at low concentrations, IZE-type MOFs displayed higher selectivity for thiophene adsorption.

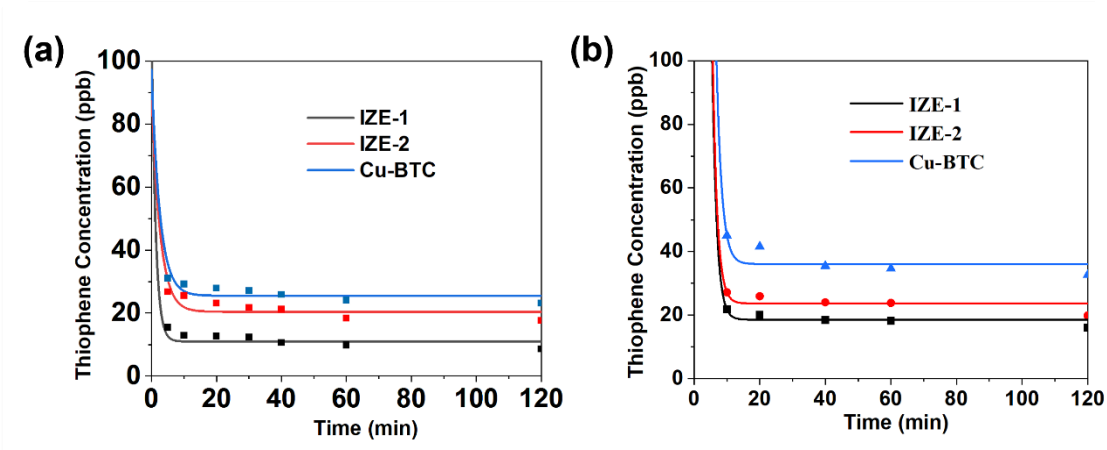

Figure 4. Under low thiophene concentration, the residual content of thiophene at different adsorption time (a) 1 ppm thiophene in thiophene/benzene mixture, (b) 17.5 ppm thiophene in thiophene/benzene mixture.

The reaction was further carried out in the thiophene/benzene mixture with

different thiophene concentrations at standard atmospheric pressure. Before the adsorption experiment, Cu-BTC and IZE MOFs were vacuum-dried overnight at 150°C to remove adsorbed water and other volatile pollutants. The experiments were carried out at 60°C with thiophene/benzene mixture of different thiophene concentrations. After 60 mins, the thiophene was almost all adsorbed to reach saturated adsorption equilibrium. Up to the 20-min mark, the three types of MOFs all showed rapid growth in adsorption capacity (Fig. 5). With thiophene/benzene mixture with 17.5 ppm thiophene, nearly all of the thiophene was by three MOFs studied (Fig. 5a). As the thiophene concentration was increased to 50 ppm, IZE-1 had higher saturated adsorption capacity of thiophene among the three MOFs, reaching 8.7 mg S/g MOF. When the thiophene concentration increased to 60 ppm, IZE-1 still has high thiophene adsorption capacity of up to 9.3 mg S/g MOF. At the same time, the thiophene adsorption capacity of IZE-2 also increased for thiophene/benzene mixture due to the increased surface area afforded by the IZE-2. Conversely, the adsorption capacity of Cu-BTC decreased for thiophene/benzene mixture with 60 ppm thiophene.

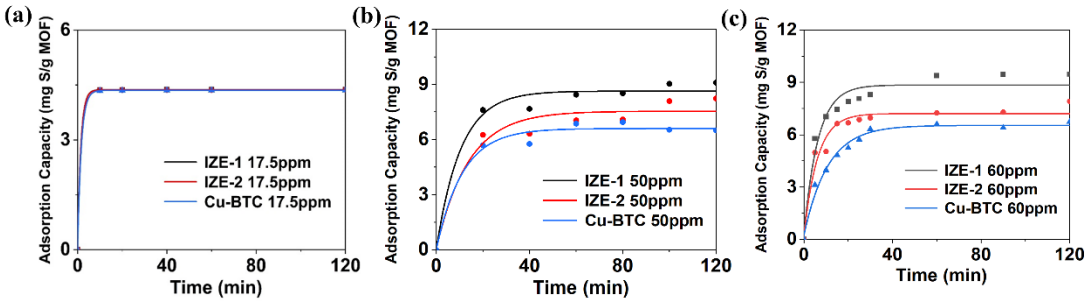

Figure 5. Under different thiophene concentration, the adsorption capacity content of thiophene as the function of time (a) 17.5 ppm thiophene in thiophene/benzene mixture, (b) 50 ppm thiophene in thiophene/benzene mixture, (c) 60 ppm thiophene in thiophene/benzene mixture.

We further studied thiophene adsorption in thiophene/benzene mixture under a wider temperature range. The thiophene adsorption capacity of different types of MOF under 40, 50, 60, and 70°C were plotted in Fig. 6a. To ensure a stable amount of thiophene adsorption, we allowed the reaction to occur for at least 120 mins shown in Fig. 6b and Fig. 6c, respectively. For Cu-BTC, the thiophene adsorption increased

rapidly during the first 20 mins, increasing slowly. The same trend was observed in IZE-1, only with a higher adsorption capacity. While IZE has higher adsorption capacity for thiophene than that of Cu-BTC (Fig. 6a). The small pore size and the electrostatic repulsion between thiophene and the carboxyl group exposed on the surface of the MOFs thus made the adsorption process difficult. The IZE-type MOF with larger pore size can increase the adsorption of thiophene at high temperature. Elevated temperature usually decreases the saturated adsorption capacity for thiophene in the MOFs. But IZE MOF showed different trend from that of Cu-BTC at high temperature. In the next section, we further investigated the difference in the the two MOF materials on the amount of thiophene adsorption as a function of temperature.

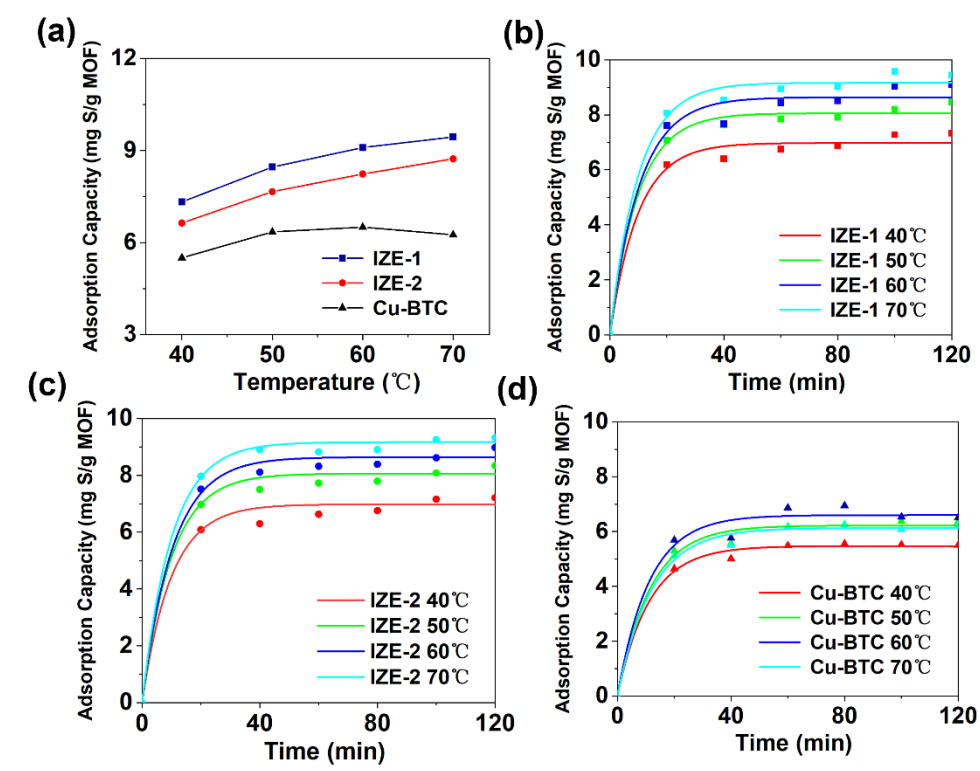

Figure 6. The adsorption capacity of thiophene at different temperatures (a) the thiophene adsorption of IZE-1, IZE-2 and Cu-BTC, (b) the thiophene adsorption of IZE-1, (c) the thiophene adsorption of IZE-2, (d) the thiophene adsorption of Cu-BTC.

4. Adsorption mechanism

To analyze the adsorption mechanism of IZE-1, we constructed the adsorption model (Figure 7a) and investigated the electronic structure of the adsorption system by first-principles simulation. We calculated the Bader charges of Zn and S atoms before

and after adsorption. The Bader charge of nearly all the S atoms after adsorption was negative, indicating that the S atoms served as electron acceptors in the process of thiophene adsorption. However, the charge density difference (Figure 7b) indicated the adsorption between OMS and S atoms to be regulated by coordination atoms, which induced adsorption deviating from the electron acceptor and donor binding mode. The partial density of states (pDOS) of OMS@S in IZE-2 before and after thiophene adsorption was calculated (Figure 7c). After adsorption, the activation of the Zn-OMS caused the isolated 3p orbital of the S atom to move towards a lower energy level, hybridizing with the Zn 3d orbital and causing Zn 3d states to move towards the Fermi level. The movement of the d orbital can be quantitatively described by D-band center theory[33] and the D-band center differences can be calculated by Eqs. (3):

$$\Delta E_d = E_b - E_a \qquad \text{Eqs. (3)}$$

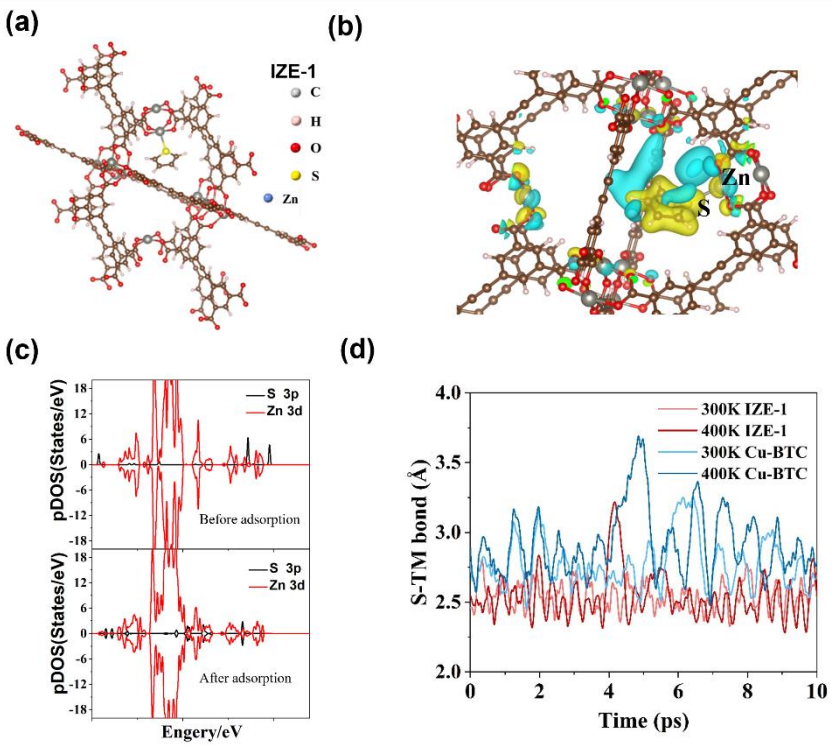

Figure 7. (a) Framework of IZE-1, (b) of Charge density of energy level in IZE-2 with thiophene adsorption, (c) Partial density of states for the change of Zn@S, (d) Variation of distances between the central metal atoms in IZE-1 and Cu-BTC and the sulfur (S) atoms in thiophene within the first 10 ps at 300 K and 400 K.

The simulation result indicates that the identity of the open metal sites can significantly affect the adsorption of thiophene. To further demonstrate the chemisorption feature of thiophene in MOFs, we studied the geometry evolution of benzene and thiophene in MOF pores by performing a molecular dynamics simulation at 300 K. The pore size of IZE-1 suggests the accommodation of 3-4 small cyclic aromatic hydrocarbons, with 6 Zn atoms possibly serving as adsorption sites. We placed one thiophene molecule and one benzene molecule in the pores for the simulation. During the long-term molecular dynamic simulation, the adsorbed molecules oscillated at the adsorption sites from 5ps to 25 ps. The distance between the S atom of thiophene and the Zn atom shrank to 0.25 nm at the 5-ps to 25-ps mark, suggesting that they chemically interacted (in Figure 8a and Figure 8b). Conversely, the benzene molecule continued reciprocating randomly within the pores, demonstrating its weak interactions with the MOF backbone. After 25 ps, the S atom of thiophene and the Zn atom of MOF always kept distance of ~0.25 nm, and the adsorption was stable (in Figure 8c). This proved the mechanism of MOF desulfurization through strong adsorption with thiophene.

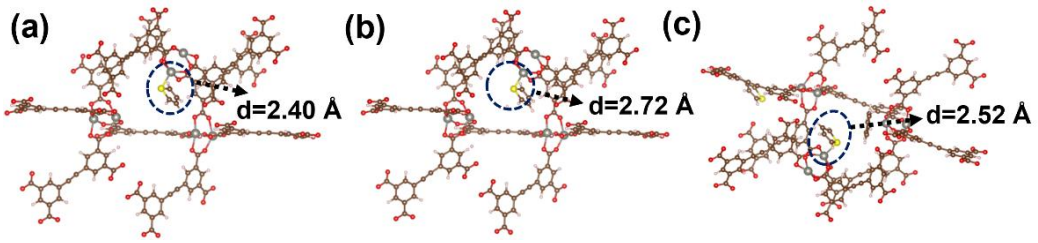

Figure 8. Molecular dynamics adsorption of thiophene and benzene in IZE-1 at 300 K with residual content of thiophene in the model. (a) 5 ps, (b) 15 ps, (c) 25 ps.

To explore the difference in thiophene adsorption behavior between Cu-BTC and IZE at higher temperatures, the adsorption energies of thiophene on IZE-1, IZE-2, and Cu-BTC were calculated. The results show that the ΔE_{ads} of IZE-1, IZE-2, and Cu-BTC are -1.24 eV, -1.19 eV, and -0.67 eV, respectively. The different behaviors observed can be attributed to the combined effect of physisorption and chemisorption. Moreover,

molecular dynamics simulations were conducted at temperatures of 300 K and 400 K to further investigate the adsorption process. The time evolution of the Zn-S and Cu-S distances within 10 ps were analyzed (Figure 7d), revealing that the distance of Cu-S is longer than that of Zn-S due to the stronger adsorption between IZE-1 and thiophene. Furthermore, the distance between metal atoms in MOFs and S atoms in thiophene is larger at 400 K compared to 300 K. However, the distance of Cu-S changes more prominently than that of Zn-S. Evidently, the adsorption of thiophene by IZE-type MOF is primarily driven by chemisorption, and its chemical reaction rate is accelerated at higher temperatures, resulting in a greater adsorption capacity. On the other hand, Cu-BTC relies more on physical adsorption for thiophene adsorption. Therefore, as the temperature increases, the adsorption capacity of Cu-BTC for thiophene weakens, as shown in Figure S6.

5. Conclusion

Adsorption performances of MOF materials with Zn and Cu metal centers are investigated both theoretically and experimentally. It is found that different metal-centered MOFs exhibited significant differences in their adsorption performance for thiophene, among which IZE-1 showed the best thiophene selectivity at low concentration and the highest thiophene adsorption capacity at high temperature. At 70°C under standard atmospheric pressure, the saturated adsorption capacity of thiophene was 9.3 mg S/g MOF. By using first-principles calculations and molecular dynamics simulations, we elucidated that the S-M bond interaction was the key factor affecting the selectivity and capacity of different metal-centers MOFs for thiophene. These results provided theoretical guidance for rationally designing and preparing efficient MOFs for removing trace thiophene from fuels.

ACKNOWLEDGMENTS

Q.Z. acknowledges the support by the Science and Technology Major Project of Hebei Province (22284402Z), the Beijing Natural Science Foundation (2192029). Z.W.S.

acknowledges the support of the Agency for Science, Technology and Research (Central Research Fund Award).

AUTHOR CONTRIBUTIONS

Yatao Wang: Validation, Funding acquisition, Formal analysis, Writing – original draft. Peng Zhang: Validation, Funding acquisition, Formal analysis, Writing – original draft. Hongjuan Li: Writing – review & editing. Qiuju Xu: The materials synthesis and electrochemical characterization. Shujun Liu: the TEM measurements. Xiaopeng Liu: Theoretical calculations. Xuehua Guo: Writing – review & editing. Yitao Li: Writing – review & editing. Jinzhang Liu: Writing – review & editing. Sen Dong: Writing – review & editing. Zhi Wei Seh: Writing – review & editing. Qianfan Zhang: Writing – review & editing.

DECLARATION OF INTERESTS

The authors declare no conflict of interest.

References

(1) Dehghan, R.; Anbia, M. Zeolites for adsorptive desulfurization from fuels: A review. *Fuel Processing Technology* **2017,** *167*, 99.

(2) Song, C. An overview of new approaches to deep desulfurization for ultra-clean gasoline, diesel fuel and jet fuel. *Catalysis Today* **2003,** *86* (1), 211.

(3) Jin, Y.; Wu, J.; Wang, J.; Fan, Y.; Zhang, S.; Ma, N.; Dai, W. Highly efficient capture of benzothiophene with a novel water-resistant-bimetallic Cu-ZIF-8 material. *Inorganica Chimica Acta* **2020,** *503*, 119412.

(4) Zu, Y.; Guan, L.; Guo, Z.; Huang, C.; He, D.; Mei, Y. Deep removal of thiophene and benzothiophene in low-sulfur fuels over the efficient CeAlSBA-15 adsorbent synthesized by sequential alumination and cerium incorporation. *Chemical Engineering Journal* **2021,** *416*, 127984.

(5) Zu, Y.; Wang, S.; Hui, Y.; Ni, N.; Zhang, X.; Qin, Y.; Zhang, L.; Liu, H.; Gao, X.; Song, L. Facile fabrication of a superior Cu(I)-NH4Y zeolite adsorbent for improving thiophene adsorption selectivity in the presence of aromatics or olefins. *Chemical Engineering Journal* **2020,** *401*, 126112.

(6) Prajapati, Y. N.; Verma, N. Adsorptive desulfurization of diesel oil using nickel nanoparticle-doped activated carbon beads with/without carbon nanofibers: Effects of adsorbate size and

adsorbent texture. *Fuel* **2017,** *189*, 186.
(7) Chen, M.; Liu, J.; Liu, Y.; Ding, Y.; Chen, J.; Yang, B.; Ma, L.; Li, L. Magnetic hybridized Fe3O4/HKUST-1 composite modified with graphite oxide to remove thiophene from model fuels. *Petroleum Science and Technology* **2019,** *37* (22), 2260.
(8) Xue, M.; Chitrakar, R.; Sakane, K.; Hirotsu, T.; Ooi, K.; Yoshimura, Y.; Feng, Q.; Sumida, N. Selective adsorption of thiophene and 1-benzothiophene on metal-ion-exchanged zeolites in organic medium. *Journal of Colloid and Interface Science* **2005,** *285* (2), 487.
(9) Yang, Y.-z.; Liu, X.-g.; Xu, B.-s. Recent advances in molecular imprinting technology for the deep desulfurization of fuel oils. *New Carbon Materials* **2014,** *29* (1), 1.
(10) Zhang, X.-F.; Wang, Z.; Feng, Y.; Zhong, Y.; Liao, J.; Wang, Y.; Yao, J. Adsorptive desulfurization from the model fuels by functionalized UiO-66(Zr). *Fuel* **2018,** *234*, 256.
(11) Hernández-Maldonado, A. J.; Yang, F. H.; Qi, G.; Yang, R. T. Desulfurization of transportation fuels by π-complexation sorbents: Cu(I)-, Ni(II)-, and Zn(II)-zeolites. *Applied Catalysis B: Environmental* **2005,** *56* (1), 111.
(12) Zu, Y.; Zhang, C.; Qin, Y.; Zhang, X.; Zhang, L.; Liu, H.; Gao, X.; Song, L. Ultra-deep adsorptive removal of thiophenic sulfur compounds from FCC gasoline over the specific active sites of CeHY zeolite. *Journal of Energy Chemistry* **2019,** *39*, 256.
(13) Li, H.; Han, X.; Huang, H.; Wang, Y.; Zhao, L.; Cao, L.; Shen, B.; Gao, J.; Xu, C. Competitive adsorption desulfurization performance over K – Doped NiY zeolite. *Journal of Colloid and Interface Science* **2016,** *483*, 102.
(14) Freund, R.; Zaremba, O.; Arnauts, G.; Ameloot, R.; Skorupskii, G.; Dincă, M.; Bavykina, A.; Gascon, J.; Ejsmont, A.; Goscianska, J.et al. The Current Status of MOF and COF Applications. *Angewandte Chemie International Edition* **2021,** *60* (45), 23975.
(15) Ding, M.; Flaig, R. W.; Jiang, H.-L.; Yaghi, O. M. Carbon capture and conversion using metal–organic frameworks and MOF-based materials. *Chemical Society Reviews* **2019,** *48* (10), 2783.
(16) Liu, X.; Wang, J.; Li, Q.; Jiang, S.; Zhang, T.; Ji, S. Synthesis of rare earth metal-organic frameworks (Ln-MOFs) and their properties of adsorption desulfurization. *Journal of Rare Earths* **2014,** *32* (2), 189.
(17) Chen, M.; Chen, J.; Liu, Y.; Liu, J.; Li, L.; Yang, B.; Ma, L. Enhanced adsorption of thiophene with the GO-modified bimetallic organic framework Ni-MOF-199. *Colloids and Surfaces A: Physicochemical and Engineering Aspects* **2019,** *578*, 123553.
(18) Chen, Z.; Zhang, P.; Wu, H.; Sun, S.; You, X.; Yuan, B.; Hou, J.; Duan, C.; Jiang, Z. Incorporating amino acids functionalized graphene oxide nanosheets into Pebax membranes for CO2 separation. *Separation and Purification Technology* **2022,** *288*, 120682.
(19) Wang, T.; Fang, Y.; Dai, W.; Hu, L.; Ma, N.; Yu, L. The remarkable adsorption capacity of zinc/nickel/copper-based metal–organic frameworks for thiophenic sulfurs. *RSC Advances* **2016,** *6* (107), 105827.
(20) Yang, L.; Lu, J.; Chen, H.; Ruckenstein, E.; Qin, Y.; Wang, T.; Sun, W.; Wang, C. Screening and Improving Porous Materials for Ultradeep Desulfurization of Gasoline. *Industrial & Engineering Chemistry Research* **2021,** *60* (1), 604.
(21) Li, Z.; Liu, S.; Liu, X.; Zhang, Q.; Lin, C.; Guo, X.; Li, Y.; Feng, X.; Dong, S.; Zhang, Q. Density functional theory screening of thiophene adsorbents and study of adsorption mechanism.

Surface Science **2022,** *721*, 122069.
(22) Chica, A.; Strohmaier, K. G.; Iglesia, E. Effects of zeolite structure and aluminum content on thiophene adsorption, desorption, and surface reactions. *Applied Catalysis B: Environmental* **2005,** *60* (3), 223.
(23) Kresse, G.; Hafner, J. Ab initio molecular dynamics for liquid metals. *Physical Review B* **1993,** *47* (1), 558.
(24) Freysoldt, C.; Grabowski, B.; Hickel, T.; Neugebauer, J.; Kresse, G.; Janotti, A.; Van de Walle, C. G. First-principles calculations for point defects in solids. *Reviews of Modern Physics* **2014,** *86* (1), 253.
(25) Blöchl, P. E. Projector augmented-wave method. *Physical Review B* **1994,** *50* (24), 17953.
(26) Hong, Y. L.; Liu, Z.; Wang, L.; Zhou, T.; Ma, W.; Xu, C.; Feng, S.; Chen, L.; Chen, M. L.; Sun, D. M.et al. Chemical vapor deposition of layered two-dimensional MoSi(2)N(4) materials. *Science* **2020,** *369* (6504), 670.
(27) Wang, S.; Zhang, L.; Zhang, M.; Xu, L.; Hu, Q.; Yang, T.; Tu, K.; Wu, M.; Yu, D. In *Water*, 2022; Vol. 14.
(28) Hao, S.; Yuling, L.; Yang, J. Synthesis of Cu-BTC by room temperature hydrothermal and its low temperature SCR denitration. *Journal of Molecular Structure* **2022,** *1251*, 132046.
(29) Zhang, J.; Shao, J.; Zhang, X.; Rao, G.; Li, G.; Yang, H.; Zhang, S.; Chen, H. Facile synthesis of Cu-BTC@biochar with controlled morphology for effective toluene adsorption at medium–high temperature. *Chemical Engineering Journal* **2023,** *452*, 139003.
(30) Hu, Y.-X.; Ma, H.-B.; Zheng, B.; Zhang, W.-W.; Xiang, S.; Zhai, L.; Wang, L.-F.; Chen, B.; Ren, X.-M.; Bai, J. Three Novel Isomeric Zinc Metal–Organic Frameworks from a Tetracarboxylate Linker. *Inorganic Chemistry* **2012,** *51* (13), 7066.
(31) Qiu, S.; Du, J.; Xiao, Y.; Zhao, Q.; He, G. Hierarchical porous HKUST-1 fabricated by microwave-assisted synthesis with CTAB for enhanced adsorptive removal of benzothiophene from fuel. *Separation and Purification Technology* **2021,** *271*, 118868.
(32) Rahman, M.; Rooney, R.; Hara, K.; Nakatani, S. Measurement of automobile N2O from bag and continuous stream by quantum cascade laser spectroscopy. *International Journal of Engine Research* **2018,** *20* (2), 261.
(33) Chen, Z.; Song, Y.; Cai, J.; Zheng, X.; Han, D.; Wu, Y.; Zang, Y.; Niu, S.; Liu, Y.; Zhu, J.et al. Tailoring the d-Band Centers Enables Co4N Nanosheets To Be Highly Active for Hydrogen Evolution Catalysis. *Angewandte Chemie International Edition* **2018,** *57* (18), 5076.